A.A. Snarskii[1,2], I.V. Bezsudnov[3,4]

[1]Dep. of general and theoretical physics, National Technical University "KPI", Kiev, Ukraine
[2]Institute for Information Recording NAS Ukraine, Kiev, Ukraine
[3]Nauka – Service JSC, Moscow, Russia
[4]ITMO University, St. Petersburg, Russia

A.A. Snarskii

I.V. Bezsudnov

THERMOELECTRIC DEVICE IN PERIODIC STEADY STATE

We propose a rotating thermoelectric (TE) device comprised of a single TE conductor operating in two periodic steady state modes: switching periodic mode (P-mode) when the hot and cold ends of the TE conductor are periodically instantly reversed and continuous sinusoidal mode (S-mode) when the temperature of TE conductor edges varies continuously according to sine wave. Power generation and cooling regimes of the rotating (TE) device in the periodic steady state were studied analytically. The efficiency and cooling temperature of the rotating TE device was found to depend not only on a dimensionless TE figure of merit, but also upon an additional dimensionless parameter comprising of the rotation period, the size and the thermal diffusivity of the TE conductor. The proposed analytical method can be generalized to even more complex timing modes and allows solving the optimization problem for TE device parameters. We investigated whether it is possible to achieve better performance for the rotating TE device comparing to conventional stationary steady state, S-mode was shown to demonstrate deeper cooling at certain times.

Key words: thermoelectric device, periodic steady state, figure of merit, power generation, cooling.

Introduction

The main way to improve the efficiency of thermoelectric (TE) devices – power generators, coolers etc. is to increase the dimensionless figure of merit of TE materials, $ZT = \alpha^2 \sigma T / \kappa$, where α is the thermopower or the Seebeck coefficient, σ is the electrical conductivity, T is the absolute temperature, κ is the thermal conductivity.

Unlike superconductivity, where new materials with high temperatures of transition to the superconducting state have been invented, the progress in ZT improvement of TE materials is quite disappointing. Thus, for example, at room temperature ($T = 300°\,\mathrm{K}$) since 1950 to the present time the figure of merit has increased from $ZT \sim 1$ to $ZT \sim 1.2 \div 1.3$ only [1-5]. Moreover, today there are no commercially available TE materials with $ZT \sim 1.3$. Indeed, for common appliances use, for example, in the household or industrial refrigeration, TE materials with the figure of merit $ZT \geq 2.0$ [6-8] are required. There were expectations that the success could be achieved using tunneling and other quantum effects in nanostructured TE materials [5, 9-13]. However, there has been no significant progress so far.

The parameters of TE device in the stationary steady state depend only on the figure of merit ZT [14]. The higher ZT, the lower cooling temperature can be reached.

In transient modes, the efficiency of TE device is affected by many other parameters, such as the temperature diffusivity, the current pulse duration in a pulsed mode [6, 15-20], the relaxation time of thermal processes etc. Such transient modes are constantly in the focus of researchers [5, 15-29],

because they have advantages over the steady state. For example, at certain times in a pulsed cooling mode [15-20] deeper cooling can be reached. Optimization of transient mode parameters allows improving the operation of TE device as compared with the steady state even if the same TE materials are used.

Qualitatively, the improved performance of TE devices in transient mode is possible due to the fact that the relaxation time of electrical processes is negligible compared to the relaxation time of thermal processes [14]. When current flows through TE device in cooling regime in the stationary steady state, the Peltier heat removed from the cold junction and the Joule heat generated in the TE conductor are balanced. Increased current and, consequently, increased Joule heat would make the TE device inoperative. In the transient state, due to the relaxation times difference, the heat balance is uncompensated. Higher current passed through the TE device for a short time delivers additional cooling. Optimization of length and shape of the current pulses can give deeper cooling for limited time intervals [18] or cooling of small objects in a shorter time [19].

The pulsed cooling [21-24] consists of two major phases. The first phase is highly transient one implementing fast and deep cooling, the second phase is the relaxation, in this phase, as a rule, the TE device is out of use. Thus, if in the pulsed mode the second phase duration is equal to or longer than the relaxation time of thermal processes (i.e. the period during which thermal equilibrium has time to be established), in the mode in hand the characteristic times (the period of change in the boundary conditions in generator mode, or current in cooling mode) are, generally speaking, shorter than the relaxation time of thermal processes.

This paper studies TE devices operating in the periodic steady state mode. Unlike pulsed cooling, a TE device in the periodic steady state mode operates continuously. The basic question considered here is whether it is possible in this periodic steady state mode to achieve better performance relative to the stationary steady state mode, at least better at certain times. In this study, we omit particular technical details such as the contact resistance of the plates, the lateral heat transfer, parameters of the cooled object etc.

The proposed TE devices consist of a single TE conductor with the constant cross section made of thermoelectric material and the role of second conductor is played by the body of TE device, which is an ordinary metal conductor.

We consider two types of periodic steady state modes for proposed TE devices: the switching periodic mode (*P*-mode) when the hot and cold ends of TE conductor are periodically instantly reversed and the continuous sinusoidal mode (*S*-mode) when the temperature of TE conductor edges varies continuously according to sine wave.

For periodic steady state modes, along with ZT we found a new dimensionless parameter that is a combination of the period of temperature change, the TE conductor size and its temperature diffusivity. The optimal value of above parameter was calculated.

In the next section, TE devices in *P*- and *S*-modes are schematically described. The following sections contain analytical calculations and results for *P*-mode in the power generation and cooling regimes, and for *S*-mode cooling regime. The last section presents discussion and conclusions.

1. Model of TE device in a periodic steady state

The TE device operating in a switching periodic mode (*P*-mode) is shown schematically in Fig. 1*a*. The TE conductor turns periodically in the plane of the figure and its hot and cold ends (junctions) are instantly swapped.

The TE device operating in a continuous sinusoidal mode (*S*-mode) is presented schematically in Fig 1*b*. Let the TE conductor rotate in the hole of the orifice plate with linear temperature distribution from up to down (see Fig. 1*b*), consequently at the ends (junctions) of the rotating TE conductor (see Fig. 1*b*) the temperature varies continuously by sine wave.

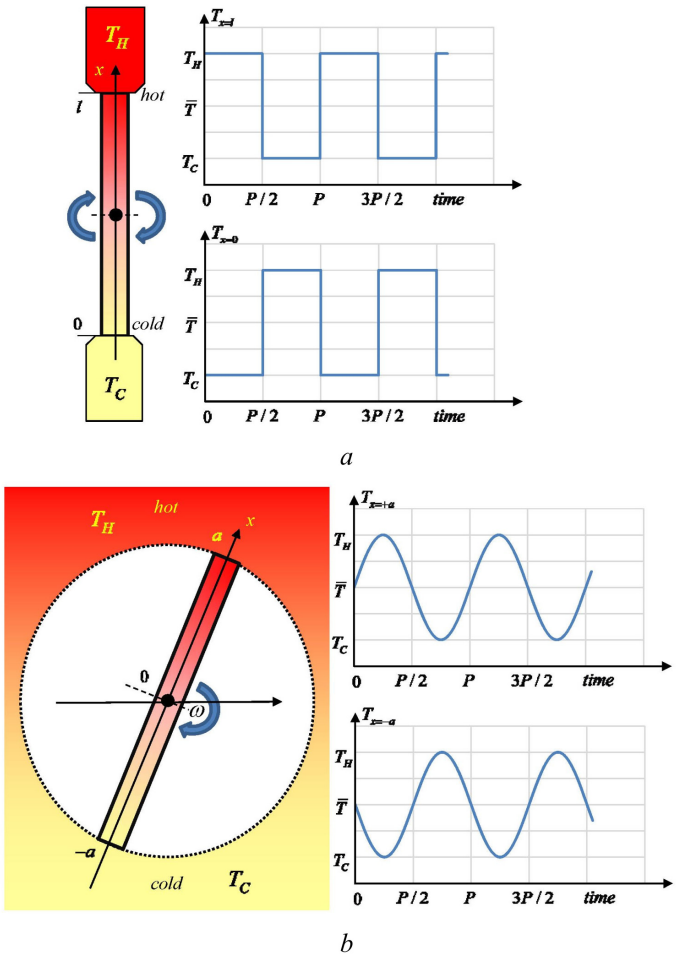

Fig. 1. Schematic sketch of proposed TE devices operating in a) the switching periodic mode (P-mode) and b) the continuous sinusoidal mode (S-mode).

The TE device (Fig. 1*a*, *b*) consists of a single TE conductor with a constant cross section S of length $l = 2a$. Other parts of TE device do not have TE properties. The period of rotation P is fixed.

Performing further analytical calculations for both *P*- and *S*-modes we assume for convenience that a TE conductor is fixed in plane but the temperature at its ends (junctions) varies according to the periodic law specific for each mode.

The heat conduction equation for the TE conductor in TE devices has the standard form [14]

$$c_v \rho_0 \frac{\partial T}{\partial t} = \kappa \frac{\partial^2 T}{\partial x^2} + \rho j^2, \qquad (1)$$

where t is the time, x is the coordinate along TE conductor, $T(x,t)$ is the temperature of TE conductor, $j(t)$ is the current density in TE conductor, $\rho = 1/\sigma$ is the specific resistivity, κ is the thermal conductivity, c_v is the specific heat, ρ_0 is the bulk density, and $\chi = \kappa / c_v \rho_0$ is the thermal diffusivity.

For *P*-mode (Fig. 1*a*) the boundary conditions are as follows

$$\begin{aligned} T(x,t)\big|_{x=0} &= \overline{T} - T_0\theta(t) \\ T(x,t)\big|_{x=l} &= \overline{T} + T_0\theta(t) \end{aligned}, \tag{2}$$

where $\overline{T}$ is the external mean temperature, T_0 is the amplitude of variation of the external temperature, the function $\theta(t)$ is set to -1 in the even half-periods and in the odd ones it is equal to $+1$

$$\theta(t) = \begin{cases} +1, & nP < t < (n+1/2)P \\ -1, & (n+1/2)P < t < (n+1)P \end{cases}. \tag{3}$$

S-mode (Fig 1*b*) corresponds to the case when the temperature of the ends (junctions) of TE conductor varies continuously according to sine wave, therefore the boundary conditions in *S*-mode are

$$T\left(x,t\right)\big|_{x=\pm a} = \overline{T} \pm T_0 \sin\left(\omega t\right), \tag{4}$$

where $\omega = P/2\pi$ is the angular frequency of temperature change, $\overline{T}$ and T_0 have the same meanings as in *P*-mode.

Thus, during the period the TE conductor in P- and S-modes has the maximum temperature at the hot end (junction) $T_H = \overline{T} + T_0$ and minimal at cold end (junction) $T_C = \overline{T} - T_0$.

The current that flows through the TE conductor in cooling regime is set to

$$\begin{aligned} j &= j_0\theta(t), && (P-\text{mode}) \\ j &= j_0 \sin\left(\frac{2\pi}{P}t\right). && (S-\text{mode}) \end{aligned} \tag{5}$$

In the power generation regime the TE conductor current is calculated according to Seebeck's law $j \sim \alpha\Delta T$, where α is the thermo power or the Seebeck coefficient, we assume it to be temperature independent

$$\begin{aligned} j &= \alpha\Delta T, \quad \Delta T = 2T_0, && (\text{P}-\text{mode}) \\ j &= \alpha\Delta T, \quad \Delta T = 2T_0 \sin\left(\frac{2\pi}{P}t\right). && (\text{S}-\text{mode}) \end{aligned} \tag{6}$$

where $2T_0 = \Delta T$ is the maximum temperature difference between the hot and cold ends (junctions).

The equation (1) with the boundary conditions (2) or (4) and the relations for the TE conductor current (5) or (6) in the periodic steady state are solved analytically in the following sections.

2. Temperature distribution and heat fluxes in the switching periodic mode (*P*-mode)

2.1. The temperature distribution in *P*-mode

The solution of the equation (1) with the boundary conditions (2) for *P*-mode was analytically calculated using the method described in [30, Chapter 15].

First, we represent $T(x,t)$ in the following form

$$T(x,t) = \overline{T} + \frac{\rho j^2}{2\kappa}x(l-x) + \tilde{T}(x,t). \tag{7}$$

Then (1) gives the equation for $\tilde{T}(x,t)$

$$\frac{\partial\tilde{T}}{\partial t} = \chi\frac{\partial^2\tilde{T}}{\partial x} \tag{8}$$

and the boundary conditions (2) become

$$\left.\tilde{T}(x,t)\right|_{x=0} = -T_0\theta(t),$$
$$\left.\tilde{T}(x,t)\right|_{x=l} = +T_0\theta(t). \tag{9}$$

Next, according to [30] we write $\tilde{T}(x,t)$ in the form of a series

$$\tilde{T}(x,t) = \sum_{k=1}^{\infty} T_k(t)\sin\frac{k\pi}{l}x\,. \tag{10}$$

Substituting $\tilde{T}(x,t)$ (10) in Eq. (8), integrating by parts twice and using the boundary conditions (9) we obtain the following relation for $T_k(t)$

$$\frac{dT_k}{dt} + \chi\left(\frac{k\pi}{l}\right)T_k = -\chi\frac{2\pi k}{l^2}T_0\theta(t)\left[1+(-1)^k\right]. \tag{11}$$

The solution of the ordinary differential equation (11) is as follows [31-33]

$$T_k(t) = T_0 e^{-A_k t} - \chi\frac{2\pi k}{l^2}\left[1+(-1)^k\right]e^{-A_k t}\int_0^t \theta(t)e^{A_k t}dt\,, \tag{12}$$

where

$$A_k = \chi\left(\frac{k\pi}{l}\right)^2. \tag{13}$$

At longer times when the periodic steady state is reached, the first transient term has to disappear.

Let $t = mP + \tau$ where $0 < \tau < P/2$ and $m >> 1$, i.e. the time τ is measured from the beginning of the period and at that time the left junction ($x = 0$) is cold and the right one ($x = l$) is hot (see Fig. 1*a*). Then, according to (3), the integral in (12) is divided into three terms, which represent the sum of odd ($\theta(t) = +1$) and even ($\theta(t) = -1$) half-periods, and the third term, which depends on τ

$$\int_0^t \theta(t)e^{A_k t}dt = \sum_{n=0}^{m}\int_{nP}^{\left(n+\frac{1}{2}\right)P} e^{A_k t}dt + -\sum_{n=0}^{m}\int_{\left(n+\frac{1}{2}\right)P}^{(n+1)P} e^{A_k t}dt + \int_{(m+1)P}^{(m+1)P+\tau} e^{A_k t}dt\,. \tag{14}$$

Calculating integrals in the first and second terms of (14) and considering $e^{-mA_k} << 1$ at $m >> 1$, we obtain geometric progressions. The sums of the above progressions we use in (12) to get the final formulae

$$T_k(\tau) = -T_0\frac{2}{k\pi}\left[1+(-1)^k\right] + 2T_0\frac{2}{k\pi}\left[1+(-1)^k\right]\frac{e^{-A_k t}}{1+e^{A_k\frac{P}{2}}}. \tag{15}$$

Substituting now (15) in (1) and considering that

$$\sum_{k=1}^{\infty}\frac{1}{k}\sin\frac{k\pi}{l}x = \frac{\pi}{2}\left(1-\frac{x}{l}\right), \tag{16}$$

we obtain

$$\tilde{T}(x,\tau) = -T_0\left(1-2\frac{x}{l}\right) + T_0\sum_{k=1}^{\infty}N_k e^{-A_k\tau}\sin\frac{k\pi}{l}x\,, \tag{17}$$

where

$$N_k = \frac{4}{k\pi}\cdot\frac{1+(-1)^k}{1-e^{A_k\frac{P}{2}}}. \tag{18}$$

Finally, the solution (1) with the boundary conditions (3) for *P*-mode has the form

$$T(x,\tau)=\overline{T}+\frac{\rho j^2}{2\kappa}x(l-x)-T_0\left(1-2\frac{x}{l}\right)+T_0\sum_{k=1}^{\infty}N_k e^{-A_k\tau}\sin\frac{k\pi}{l}x, \qquad (19)$$

where τ belongs to $[0\ldots P/2]$.

Fig. 2 shows the temperature distribution along the TE conductor in *P*-mode at different times.

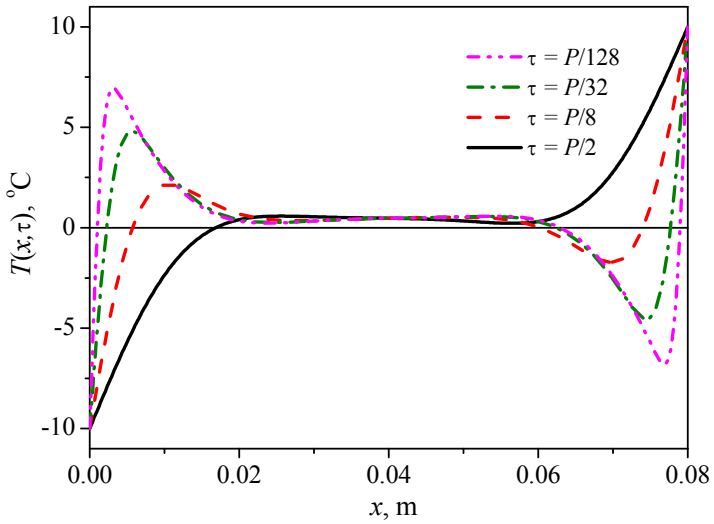

Fig. 2. Temperature distribution of TE conductor in P-mode at different times measured from the beginning of the period $P/128...P/2$. External temperatures: $\overline{T}=0°C$, $T_0=10°C$, TE conductor length $l=0.08\,m$, TE material parameters $\kappa=1.7\,W/mK$, $\chi=1.2\cdot10^{-6}\,m^2/s$, current density $j=0.1\cdot10^6\,A/m^2$ and rotation period $P=1s$.

At $t=P,\ 2P,\ 3P,\ldots$ the temperature of TE conductor edges is changing instantly. Then after this leap the TE conductor starts warming up, it is clearly seen from Fig. 2, but there is still part of TE conductor with the temperature $T(x,\tau)<\overline{T}$. Eventually, the size of this part decreases and its temperature increases.

Selected TE conductor and operational parameters show the case when temperature in the middle of the TE conductor is stable, i.e. heat waves do not enter deeply the TE conductor. It is similar to permafrost, when a periodic variation of the temperature on Earth's surface does not affect the temperature at a certain depth.

It should be noted also that the temperature in the middle of TE conductor is slightly higher than $\overline{T}$ because of the emitted Joule heat. When no current flows the temperature in the center of TE conductor, of course, would be equal to $\overline{T}$.

2.2. Power generation efficiency in *P*-mode

The power generation efficiency η of TE device in P-mode depends on the heat flux coming into the hot junction and coming out of the cold junction of the TE conductor (at $x=0$ and $x=l$ respectively) [14]. The heat flux density q_x is the sum of the flux densities created by the temperature distribution $\sim\partial T/\partial x$ and the Peltier heat flux $\Pi\mathbf{j}$, where $\Pi=\alpha T$ is the Peltier coefficient (we assume that the thermoEMF or the Seebeck coefficient α is temperature independent).

$$q_x=-\kappa\frac{\partial T}{\partial x}-\alpha Tj\ . \qquad (20)$$

We find the heat flux at cold $\dot{Q}_C$ and hot $\dot{Q}_H$ junctions using (19)

$$\dot{Q}_C = q_x S\big|_{x=0} = -\frac{\rho J^2}{2}\frac{l}{S} - \kappa\frac{2T_0}{l}S - \kappa T_0 S\sum_{k=1}^{\infty}\frac{k\pi}{l}N_k e^{-A_k\tau} + \alpha T_c J\,, \tag{21}$$

$$\dot{Q}_H = q_x S\big|_{x=l} = -\frac{\rho J^2}{2}\frac{l}{S} - \kappa\frac{2T_0}{l}S - \kappa T_0 S\sum_{k=1}^{\infty}(-1)^k\frac{k\pi}{l}N_k e^{-A_k\tau} + \alpha T_H J\,. \tag{22}$$

Here S is the cross section of TE conductor, J is the current flows through TE conductor. J is governed by the ε generated according to the Seebeck effect $\varepsilon = \alpha(T_H - T_C)$ and by connected in series the TE conductor resistance $r = \rho l / S$ and the load resistance R:

$$J = \alpha\frac{T_H - T_C}{r + R} = \alpha\frac{2T}{r(1+\Omega)}, \qquad \Omega = \frac{r}{R}\,. \tag{23}$$

The signs of the Peltier heat terms in (21) and (22) are selected in the way that the flux positive direction is from the hot to cold junction i.e. the heat flux coming to the hot junction ($x = l$) and coming out of the cold ($x = 0$) junction is set to be positive.

The heat coming out of the hot Q_H and coming to the cold Q_C junctions depends on time, therefore to get the efficiency η, we have to integrate Q_H and Q_C for a certain time, such time for *P*-mode is $P/2$ – half of the period:

$$Q_H = \int_0^{P/2}\dot{Q}_H d\tau, \qquad Q_C = \int_0^{P/2}\dot{Q}_C d\tau\,. \tag{24}$$

Substituting in (24) the expressions for $\dot{Q}_H$ (21) and $\dot{Q}_C$ (22) we find

$$\left.\begin{aligned}\frac{1}{P/2}Q_C &= \frac{1}{2}rJ^2 + \frac{2T_0}{l}S\kappa_e + \alpha T_c J\\ \frac{1}{P/2}Q_H &= -\frac{1}{2}rJ^2 + \frac{2T_0}{l}S\kappa_e + \alpha T_H J\end{aligned}\right\}, \tag{25}$$

where the renormalized thermal conductivity is

$$\kappa_e = \kappa\left[1 + \frac{4\mu_0^2}{\pi}\sum_{k=1}^{\infty}\frac{1+(-1)^k}{(k\pi)^2}th\left(A_k\frac{P}{4}\right)\right] \tag{26}$$

and

$$\mu_0^2 = l^2\frac{1}{P\chi}\,. \tag{27}$$

Comparing the relations (25) and (26) for *P*-mode and the formulae for the stationary steady state [14], one can realize that they differ only in the thermal conductivity value. The efficiency η in the stationary steady state depends only on the thermal conductivity κ, but in *P*-mode it depends upon the renormalized thermal conductivity κ_e (26) which is a complex parameter proportional not only to the TE conductor thermal conductivity κ, but also to the length of TE conductor, the switching period P and the thermal diffusivity χ.

Therefore, the corresponding expression for the efficiency $\eta = (Q_H - Q_C)/Q_H$ for *P*-mode is similar to the stationary steady state but it uses the renormalized thermal conductivity κ_e (26). The appropriate calculations can be found for instance in [14] and below is the final expression

$$\eta = \frac{Z_e \Delta T \Omega}{(1+\Omega)^2 \left[1 + \frac{Z_e T_H}{1+\Omega} - \frac{1}{2} \frac{Z_e \Delta T}{(1+\Omega)^2} \right]}, \tag{28}$$

where $Z_e = \sigma\alpha^2 / \kappa_e$ is a dimensionless TE figure of merit renormalized using (26).

As in the stationary steady state [14], the maximum efficiency η in *P*-mode is achieved at the optimal ratio $\Omega_{opt} = R / r = \sqrt{1 + Z_e \overline{T}}$. Using Ω_{opt} in (28) we find the value of maximal efficiency $\eta_{\max}$ for *P*-mode that depends only on T_H, T_C and Z_e

$$\eta_{\max} = \frac{\Delta T}{T_H} \frac{\sqrt{1 + Z_e \overline{T}} - 1}{\sqrt{1 + Z_e \overline{T}} - \frac{T_C}{T_H}} . \tag{29}$$

The maximum efficiency $\eta_{\max}$ is a monotonically increasing function of Z_e, thus higher Z_e and, accordingly, lower κ_e yields a better $\eta_{\max}$ value.

The renormalized thermal conductivity κ_e in *P*-mode (26) is always greater than κ, $\kappa_e > \kappa$, thus the efficiency in *P*-mode (28) is always less than the efficiency in the stationary steady state. In the case, when $\chi P \pi^2 / 4l > 3$, the hyperbolic tangent in (26) is nearly one and considering $\sum_{k=1}^{\infty} \left[\left(1 + (-1)^k\right) \Big/ \left(k\pi\right)^2 \right] = 1/12$ we get the approximated expression for the renormalized thermal conductivity

$$\kappa_e \approx \kappa \left(1 + \frac{1}{3} {\mu_0}^2 \right). \tag{30}$$

To have the efficiency of TE device in P-mode as high as possible, we need $\kappa_e \to \kappa$ or $\mu_0^2 \to 0$ (30). The latter means higher χ values or shorter lengths l of the TE conductor. In other words, for half of the period the TE conductor has to be warmed almost as the TE conductor in the stationary steady state.

2.3. Cooling in *P*-mode

Calculations for the cooling regime in *P*-mode are similar to those for the efficiency, except that it must be borne in mind that the current is determined by (5) $J = J_0 \theta(t)$ rather than by the Seebeck effect. The optimal current J_{opt} will minimize the cooling temperature or maximize the coefficient of performance K.

The heat fluxes $\dot{Q}_C$ and $\dot{Q}_H$ in *P*-mode cooling regime differ from (21) and (22) only by the signs of the Peltier heat term because the current in the TE conductor flows in the direction opposite to power generation regime.

$$\left.\begin{aligned} \frac{1}{P/2} Q_C &= \frac{1}{2} r J^2 + \frac{2T_0}{l} S\kappa_e - \alpha T_C J \\ \frac{1}{P/2} Q_H &= -\frac{1}{2} r J^2 + \frac{2T_0}{l} S\kappa_e - \alpha T_H J \end{aligned}\right\}. \tag{31}$$

In cooling regime, we have to follow variations of the effective (normalized) thermal conductivity $\kappa_e(\tau)$ to find the time when the lowest possible cooling temperature can be reached. $\kappa_e(\tau)$ depends on the time τ as follows

$$\kappa_e(\tau) = \kappa\left[1 + \frac{1}{2}\sum_{k=1}^{\infty} k\pi N_k e^{-A_k\tau}\right]. \tag{32}$$

It should be noted that $\kappa_e(\tau)$ in contrast to κ_e (26) does not use the factor μ_0^2 (27).

Next, as in the stationary steady state, the condition $\partial\dot{Q}_C / \partial J = 0$ for the current gives

$$J_{opt} = \frac{\alpha T_C}{\rho l} S = \frac{\alpha T_C}{r}. \tag{33}$$

Note that in contrast to the stationary steady state, the thermo conductivity $\kappa_e(\tau)$ (32) depends on the time τ, however, it does not affect the value of the optimal current J_{opt}.

The expression for the heat flux at the cold junction at the optimum current is equal to

$$\frac{1}{S}\dot{Q}_C = -\frac{1}{2}\frac{\alpha^2 T_C^2}{\rho l} + \frac{2T_0}{l}\kappa_e(\tau) \tag{34}$$

In the stationary steady state, the minimum cooling temperature $T_C^{\min}$ is found from the condition $\dot{Q}_C = 0$. In P-mode the condition $\dot{Q}_C = 0$ is only possible at certain times. Assuming $\dot{Q}_C = 0$ (34) we get

$$T_C^{\min} = 2\overline{T}\frac{\sqrt{1 + Z_e(\tau)\overline{T}} - 1}{Z_e(\tau)\overline{T}}, \tag{35}$$

where the renormalized figure of merit $Z_e(\tau) = \sigma\alpha^2 / \kappa_e(\tau)$ depends on the time τ.

The only difference between $T_C^{\min}(\tau)$ (35) and the expression for $T_C^{\min}$ in the stationary steady state is the value of figure of merit. The $T_C^{\min}(\tau)$ (35) uses the renormalized thermal conductivity $\kappa_e(\tau)$ which depends on the time τ and allows optimization of cooling temperature.

The $Z_e(\tau)$ maximum value, i.e. the minimum cooling temperature $T_C^{\min}$ corresponds to the minimum $T_C^{\min}$. As it follows from (32), $\kappa_e(\tau)$ has a minimum at $\tau = P/2$, however, even in this case $\kappa_e(\tau = P/2) > \kappa$ i.e. similar to *P*-mode power generation regime.

Due to the fact that $\kappa_e(\tau) > \kappa$, the coefficient of performance $K = \dot{Q}_C / \left(\dot{Q}_H - \dot{Q}_C\right)$ and the maximum cooling capacity $Q_C^{\max}$ are less than those in the stationary steady state, although at certain values of the thermo conductivity, the switching period and other TE conductor parameters are close to it.

The above conclusions apply only to *P*-mode. Further, we show that the TE device operating in *S*-mode can demonstrate a better performance.

3. Temperature distribution and heat flux in *S*-mode

3.1. The temperature distribution in *S*-mode

The solution of the equation (1) with the boundary conditions (4) for *S*-mode begins from representing $T(x,t)$ in the form

$$T(x,t) = \overline{T} - j_0^2 F\left(\sin 2\omega t - \mu^2\frac{a^2 - x^2}{a^2}\right) + \tilde{T}(x,t), \tag{36}$$

where

$$\mu^2 = a^2 \frac{\omega}{\chi}\ ,\ F = \frac{\rho}{4c_v \rho_0 \omega}. \tag{37}$$

Then (1) gives the equation for $\tilde{T}(x,t)$

$$\frac{\partial \tilde{T}}{\partial t} = \chi \frac{\partial^2 \tilde{T}}{\partial x^2} \tag{38}$$

and the boundary condition (4) becomes

$$\tilde{T}(x,t)\Big|_{x=\pm a} = \pm T_0 \sin(\omega t) + j_0^{\,2}\,\mathrm{F}\sin(2\omega t). \tag{39}$$

The solution of (38) with the boundary conditions can be found in the form

$$\tilde{T}(x,t) = T_0\left(S(x)\sin\omega t + C(x)\cos\omega t\right) + j_0^{\,2}\,\mathrm{F}\left(\tilde{S}(x)\sin 2\omega t + \tilde{C}(x)\cos 2\omega t\right), \tag{40}$$

where

$$\begin{cases} S(x) = S_{cs}\,\mathrm{ch}\left(\frac{\mu}{\sqrt{2}a}x\right)\sin\left(\frac{\mu}{\sqrt{2}a}x\right) + S_{sc}\,\mathrm{sh}\left(\frac{\mu}{\sqrt{2}a}x\right)\cos\left(\frac{\mu}{\sqrt{2}a}x\right), \\ C(x) = S_{sc}\,\mathrm{ch}\left(\frac{\mu}{\sqrt{2}a}x\right)\sin\left(\frac{\mu}{\sqrt{2}a}x\right) - S_{cs}\,\mathrm{sh}\left(\frac{\mu}{\sqrt{2}a}x\right)\cos\left(\frac{\mu}{\sqrt{2}a}x\right), \\ \tilde{S}(x) = \tilde{S}_{cc}\,\mathrm{ch}\left(\frac{\mu}{a}x\right)\cos\left(\frac{\mu}{a}x\right) + \tilde{S}_{ss}\,\mathrm{sh}\left(\frac{\mu}{a}x\right)\sin\left(\frac{\mu}{a}x\right), \\ \tilde{C}(x) = -\tilde{S}_{ss}\,\mathrm{ch}\left(\frac{\mu}{a}x\right)\cos\left(\frac{\mu}{a}x\right) + \tilde{S}_{cc}\,\mathrm{sh}\left(\frac{\mu}{a}x\right)\sin\left(\frac{\mu}{a}x\right). \end{cases} \tag{41}$$

The boundary conditions (39) allow finding coefficients in (41):

$$\begin{aligned} S_{cs} &= \frac{\mathrm{ch}(\mu/\sqrt{2})\sin(\mu/\sqrt{2})}{\mathrm{sh}^2(\mu/\sqrt{2}) + \sin^2(\mu/\sqrt{2})},\ S_{sc} = \frac{\mathrm{sh}(\mu/\sqrt{2})\cos(\mu/\sqrt{2})}{\mathrm{sh}^2(\mu/\sqrt{2}) + \sin^2(\mu/\sqrt{2})}, \\ \tilde{S}_{ss} &= \frac{\mathrm{sh}(\mu)\sin(\mu)}{\mathrm{ch}^2(\mu) - \sin^2(\mu)}, \qquad \tilde{S}_{cc} = \frac{\mathrm{ch}(\mu)\cos(\mu)}{\mathrm{ch}^2(\mu) - \sin^2(\mu)}. \end{aligned} \tag{42}$$

Therefore, the solution of (1) with the boundary conditions (4) can be written as

$$\begin{aligned} T(x,t) = \overline{T} + T_0\left(S(x)\sin\omega t + C(x)\cos\omega t\right) + \\ + j_0^{\,2}\,\mathrm{F}\left(\sin 2\omega t + \mu^2\frac{a^2 - x^2}{a^2} + \tilde{S}(x)\sin 2\omega t + \tilde{C}(x)\cos 2\omega t\right). \end{aligned} \tag{43}$$

The solution $T(x,t)$ (43) includes both the terms proportional to $\sin\omega t$, $\cos\omega t$ and those proportional to $\sin 2\omega t$, $\cos 2\omega t$ – double the frequency of the temperature change at the TE conductor ends (junctions). The terms in (43) with $\sin\omega t$ and $\cos\omega t$ owe their origin to the heat flux generated by the temperature difference at the TE conductor ends ($x = \pm a$), their amplitude is proportional to T_0. Such terms describe common temperature waves damping with the distance from TE conductor ends ($x = \pm a$). Parameter μ^2 is a combination of the frequency, the length and the thermal diffusivity of TE conductor which is similar to μ_0^2 in *P*-mode(27).

The double frequency terms $\sin 2\omega t$, $\cos 2\omega t$ in (43) are proportional to the square of the amplitude of the current density amplitude j_0^2. Those terms describe the heat flux, born by the heterogeneity of the temperature distribution due to the Joule heat.

In Fig 3 we present the temperature distribution in the TE conductor which has the same parameters as in Fig. 2 above, but used in *S*-mode.

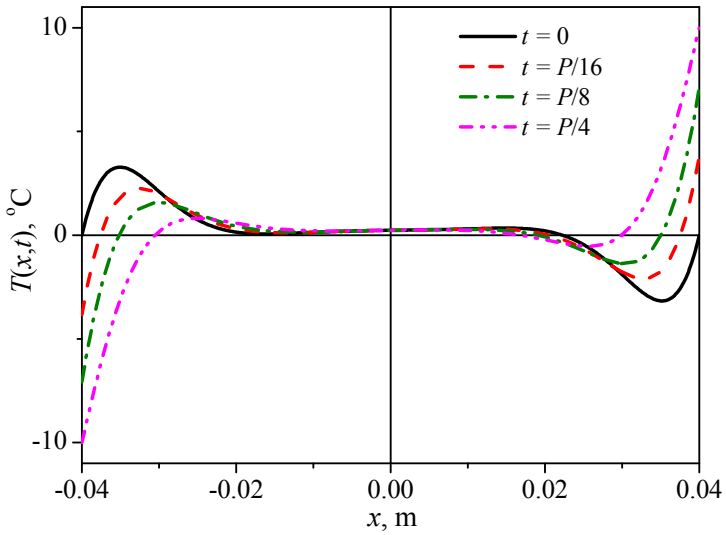

Fig. 3. Temperature distribution of TE conductor in S-mode at different times measured from the beginning of the period: $0...P/16$. External temperatures: $\bar{T} = 0\,°C$, $T_0 = 10\,°C$, TE conductor size $a = 0.04\ m$, TE material parameters $\kappa = 1.7\ W/mK$, $\chi = 1.2 \cdot 10^{-6}\ m^2/s$, current density amplitude $j = 0.1 \cdot 10^6\ A/m^2$ and rotation period $P = 1s$.

Fig. 3 shows that the temperature distribution of TE conductor in *S*-mode is similar to that for *P*-mode. But the temperature at the TE conductor edges in *S*-mode is changed continuously by sine wave in the range $\bar{T} \pm T_0$. In the center of the TE conductor $T(0,t) > \bar{T}$ because of the Joule heat emission.

3.2. Cooling in *S*-mode

Let during the first half-period the TE conductor has the lower end (junction) temperature (see Fig. 1*b*) colder than upper one, i.e. the lower junction is cold one.

Therefore, the heat flux at the cold junction $(x = -a)$ is

$$Q_C = -q_x S\big|_{x=-a} = S\kappa \frac{\partial T}{\partial x}\bigg|_{x=-a} - \alpha T_C(t) j(t) S\,, \tag{44}$$

where the second term is the Peltier heat flux, S is the cross section of TE conductor, $T_C(t) = T(x = -a, t)$.

Substituting in (44) the expression for the temperature distribution from (43) at $x = -a$ we obtain

$$\begin{aligned} \frac{Q_C}{S}\bigg|_{x=-a} &= \kappa T_0 \left(S'(-a)\sin\omega t + C'(-a)\cos\omega t \right) + \\ &+ \kappa j_0^{\,2}\,\mathrm{F}\left(-\frac{2\mu^2}{a} + \tilde{S}'(-a)\sin 2\omega t + \tilde{C}'(-a)\cos 2\omega t \right) - \alpha T_C(t) j(t), \end{aligned} \tag{45}$$

where S', C', S', C' are the derivatives with respect to coordinate at $x = -a$.

At the cold junction according to (4) the temperature will be minimal at $\omega t = \pi/2$. We denote it as T_c. At that moment the heat flux at the cold junction is

$$\frac{Q_C}{S}\bigg|_{\substack{x=-a \\ \omega t=\pi/2}} = \kappa T_0 S'(-a) - \kappa j_0^{\,2}\,\mathrm{F}\left(2\mu^2/a - \tilde{C}'(-a)\right) - \alpha T_C j_0\,. \tag{46}$$

To determine the lowest possible cooling temperature of the cold junction, we have to find the minimum of the heat flux at the cold junction i.e. $Q_C / S \left|_{\substack{x=-a \\ \omega t=\pi/2}}\right.$ as the function of current density amplitude j_0, then to find the optimal current j_0^{opt} we use the condition $\partial Q_C / \partial j_0 = 0$. Further, using j_0^{opt} we calculate the heat flux at the cold junction (46) and finally obtain the minimal cooling temperature $T_C^{\min}$.

The optimal current value j_0^{opt} is

$$j_0^{opt} = \frac{\alpha T_C}{2\mathrm{F}\kappa\left(2\mu^2 / a - \tilde{C}'(-a)\right)}. \tag{47}$$

At the minimal temperature $T_C^{\min}$ the heat flux Q_C of the cold junction at the current density amplitude j_0^{opt} to be equal to zero

$$\left.\frac{Q_C}{S}\right|_{\substack{x=-a \\ \omega t=\pi/2}} = \kappa T_0 S'(-a) - \frac{(\alpha T_C)^2}{4\mathrm{F}\kappa}\frac{1}{\left(2\mu^2 / a - \tilde{C}'(-a)\right)} = 0. \tag{48}$$

Using $T_0 = \overline{T} - T_C$ for (48) we find

$$T_C^2 = 2\overline{T}(\overline{T} - T_C)\left[\frac{2F\kappa^2}{\overline{T}\alpha^2 a^2}\left(2\mu^2 - a\tilde{C}'(-a)\right)aS'(-a)\right]. \tag{49}$$

Let us denote the term in square brackets in (49) $\beta(\mu, Z\overline{T}) / Z\overline{T}$ then using $2F\kappa^2 / \overline{T}\alpha^2 a^2 = 1/2Z\overline{T}\mu^2$ we write the following formulae for the dimensionless parameter $\beta(\mu)$

$$\begin{aligned}\beta(\mu) = \frac{\mu}{2\sqrt{2}}\left(1 + \frac{1}{2\mu}\frac{\mathrm{sh}(\mu)\mathrm{ch}(\mu) + \cos(\mu)\sin(\mu)}{\mathrm{ch}^2(\mu) - \sin^2(\mu)}\right)\times \\ \times \frac{\mathrm{sh}(\mu/\sqrt{2})\mathrm{ch}(\mu/\sqrt{2}) + \sin(\mu/\sqrt{2})\cos(\mu/\sqrt{2})}{\mathrm{sh}^2(\mu/\sqrt{2}) + \sin^2(\mu/\sqrt{2})}\end{aligned} \tag{50}$$

and the equation (49) is rewritten in the form

$$T_C^{\,2} + \frac{\beta(\mu)}{Z\overline{T}}\overline{T}T_C - \frac{\beta(\mu)}{Z\overline{T}}\overline{T}^2 = 0. \tag{51}$$

To calculate $T_C^{\min}$ we have to solve the quadratic equation (51), the positive root of (51) gives $T_c^{\min}$

$$T_C^{\min} = \frac{2\overline{T}}{1 + \sqrt{1 + \frac{Z\overline{T}}{\beta(\mu)}}}. \tag{52}$$

Let us compare $T_C^{\min}$ in *S*-mode to the minimal cooling temperature in the stationary steady state T_C^{st} that can be expressed [14] as follows

$$T_C^{st} = \frac{T_H}{\sqrt{1 + Z\overline{T}}}, \tag{53}$$

or using $T_H = 2\overline{T} - T_C$

$$T_C^{st} = \frac{2\overline{T}}{1 + \sqrt{1 + Z\overline{T}}}. \tag{54}$$

Relations (52) and (54) have the similar form that allows rewriting the expression for $T_c^{\min}$

$$T_C^{\min} = \frac{2\overline{T}}{1+\sqrt{1+Z_e\overline{T}}}, \tag{55}$$

where $Z_e\overline{T}$ is the renormalized figure of merit

$$Z_e\overline{T} = \frac{Z\overline{T}}{\beta(\mu)}. \tag{56}$$

Thus, *S*-mode calculations are also similar to the stationary steady state. As seen from (55) $T_C^{\min}$ is a monotonically increasing function of the dimensionless parameter $\beta(\mu)/Z\overline{T}$, at large values $\beta(\mu)/Z\overline{T} >> 1$ we obtain $T_C^{\min} \to \overline{T}$, that means no cooling at large $\beta(\mu)/Z\overline{T}$, i.e. the smaller the value $\beta(\mu)/Z\overline{T}$, the lower $T_C^{\min}$.

Also we can state that the higher TE figure of merit $Z\overline{T}$ means better cooling in *S*-mode (50) and opposite, when $Z\overline{T} \to 0$, $\beta(\mu)/Z\overline{T} \to \infty$ and the cooling is impossible. Further, note that (50) и (52) show that $T_C^{\min}$ depends only on the single dimensionless parameter – μ.

Let examine the ratio of minimal temperatures in *S*-mode and in the stationary steady state

$$\frac{T_C^{\min}}{T_C^{st}} = \frac{1+\sqrt{1+Z_e\overline{T}}}{1+\sqrt{1+Z\overline{T}}} = \frac{1+\sqrt{1+Z\overline{T}/\beta(\mu)}}{1+\sqrt{1+Z\overline{T}}}. \tag{57}$$

When the figure of merit $Z\overline{T}$ is fixed, the ratio (57) depends only on the single parameter $\beta(\mu)$. The function $\beta(\mu)$ has one minimum and it is invariant relative to $Z\overline{T}$. The minimum is at $\mu \approx 1.53$ and accordingly $\beta \approx 0.76 < 1$ i.e. the TE device in S-mode will deliver deeper cooling at certain times than in the stationary steady state (see Fig. 4).

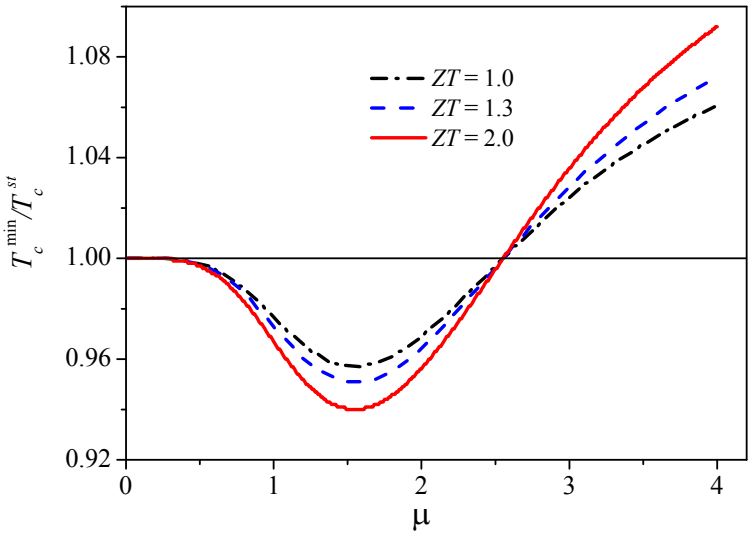

Fig. 4. Ratio of minimal temperatures T_c^{min}/T_c^{st} *for S-mode and stationary steady state on* μ *for* $Z\overline{T} = 1.0, 1.4, 2.0$.

As an example, for the TE device in *S*-mode with the TE conductor made of Bi_2Te_3 [34] (the temperature diffusivity $\chi \approx 1.2 \cdot 10^{-6}$ m^2/s) we choose the length of the TE conductor $2a = 1.5$ mm and the rotation period $P \approx 1.15$ s that gives optimal $\mu_{\min} \approx 1.53$.

For TE device operating in *S*-mode with the above parameters, we calculated $T(x,t)$, measured from the beginning of the period – Fig. 5.

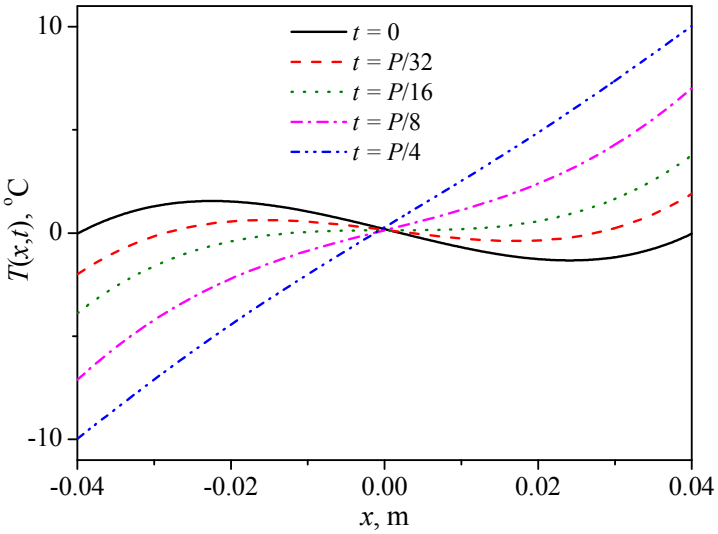

Fig. 5. Temperature distribution of TE conductor in S-mode at different times measured from the beginning of the period: $0...P/32$. *External temperatures:* $\overline{T} = 0°C$, $T_0 = 10°C$, *TE material dimensionless parameter* $\mu_{min} \approx 1.53$, *TE conductor size* $a = 0.04\,m$.

Comparison of Fig. 3 and Fig. 5 shows that exactly at a critical value of the dimensional parameter equal to $\mu_{min} \approx 1.53$ the coordinate dependence of $T(x,t)$ at time moment $P/4$ becomes linear, the heat penetrates to the middle of the leg and, thus, its entire volume is fully operated.

For *S*-mode at optimal $\beta(\mu) \approx 0.76$ the minimal achievable cooling temperature can be expressed as

$$T_c^{\min} \approx \frac{2\overline{T}}{1+\sqrt{1+1.3Z\overline{T}}}. \tag{58}$$

In other words, using the TE material with $ZT = 1$ in S-mode, we get cooling as of material with $ZT = 1.3$ in the stationary steady state. The TE material with $ZT = 1.3$ in *S*-mode corresponds to $ZT = 1.7$ in the stationary steady state.

4. Discussion and conclusions

The paper describes two types of proposed TE device that operate in periodic steady state modes: *P*-mode – the switching periodic mode and *S*-mode – the continuous sinusoidal mode.

In common, the efficiency of TE device is related to the rate of entropy production or particularly to the volume integral of the divergence of the entropy flux density $\mathbf{s} = \mathbf{q}/T$, $B = \int_V div(\mathbf{s})dV$. Finally, the efficiency can be written in the form

$$\eta = \eta_c \frac{1}{1+\frac{BT_H}{A}}, \tag{59}$$

where A is the work performed by the TE power generator.

Thus, the higher entropy production rate, the lower the efficiency of TE device in the power generation regime. Transient regimes, having some additional spatial inhomogeneity of the temperature distribution, naturally lead to the additional entropy production B and, as a consequence, the efficiency has to be even lower.

But the relation (59) that binds the efficiency and the entropy production is derived for the stationary steady state. Therefore, to predict what could be the efficiency in transient, pulsed or periodic modes is almost impossible in advance. Generally, the article discusses the possible benefits of TE device usage in transient modes, particularly periodic modes.

S-mode was shown to demonstrate deeper cooling at certain times, as compared with the stationary steady state.

The proposed method to calculate analytically parameters of TE devices in periodic *P*- and *S*-modes for the power generation regime or the cooling regime can be generalized to even more complex timing modes. The analytical solution allows applying the optimization technique to find optimal TE device parameters.

Acknowledgments

Authors would like to express their great appreciation to Dr. L.N. Vikhor, Prof. S.Z. Sapozhnikov, and Prof. I.V. Andrianov for their valuable and constructive suggestions during development of this research work.

I.V.Bezsudnov was supported by the Government of the Russian Federation (Grant 074-U01).

Appendix A

Solution of thermal conductivity equation in *P* – mode

Here we cite a solution of temperature distribution problem (1) with the boundary conditions (2) in *P* – mode (see Fig. 1) using a standard method of separation of variables.

As above in the text of the paper, for thermoelement leg in time intervals from nP to $(n+1)P/2$, where P is a period, and $n = 0, 1, ...$ the lower end is cold, and the upper end is hot.

We assume, as before, $l = 2a$, and re-write the thermal conductivity equation (1), the boundary conditions (2), just as substitution of variables, made in (7) in coordinates $x = -a...a$.

Thermal conductivity equation

$$\frac{\partial T}{\partial t} = \chi \frac{\partial^2 T}{\partial x^2} + \frac{\rho}{c_V \rho_0} j^2, \tag{A1}$$

and the boundary conditions

$$T\big|_{x=\pm a} = \overline{T} + T_0 \theta(t). \tag{A2}$$

Substituting

$$T(x,t) = \overline{T} + \frac{\rho j^2}{\kappa}\left(a^2 - x^2\right) + \tilde{T}(x,t), \tag{A3}$$

we obtain

$$\frac{\partial \tilde{T}}{\partial t} = \chi \frac{\partial^2 \tilde{T}}{\partial t^2}, \tag{A4}$$

$$\tilde{T}(x,t)\big|_{x=\pm a} = T_0 \theta(t). \tag{A5}$$

Let us represent the solution of equation (A1) with the boundary conditions (A2) in the form

$$T(x,t)=\overline{T}+\frac{\rho j^2}{\kappa}\left(a^2-x^2\right)+\tilde{T}(x,t)=\overline{T}+\frac{\rho j^2}{\kappa}\left(a^2-x^2\right)+ T_0\sum_{n=1}^{\infty}b_n\left[S_n(x)\sin\left(\frac{2\pi}{P}nt\right)+C_n(x)\cos\left(\frac{2\pi}{P}nt\right)\right], \tag{A6}$$

where

$$C_n(x)=\frac{1}{\Omega_n}\left[B_n\,\mathrm{ch}(\lambda_n x)\sin(\lambda_n x)-A_n\,\mathrm{sh}(\lambda_n x)\cos(\lambda_n x)\right],$$
$$S_n(x)=\frac{1}{\Omega_n}\left[A_n\,\mathrm{ch}(\lambda_n x)\sin(\lambda_n x)+B_n\,\mathrm{sh}(\lambda_n x)\cos(\lambda_n x)\right],\quad \lambda_n=\sqrt{n\pi/\chi P}. \tag{A7}$$

Coefficients A_n, B_n and Ω_n are as follows

$$A_n=\mathrm{ch}(\lambda_n a)\sin(\lambda_n a),\qquad B_n=\mathrm{sh}(\lambda_n a)\cos(\lambda_n a),\qquad \Omega_n=A_n^2+B_n^2, \tag{A8}$$

and b_n is coefficient of $\theta(t)$ expansion into a Fourier series.

$$\theta(t)=\sum_{n=1}^{\infty}b_n\sin\left(\frac{2\pi}{P}nt\right),\qquad b_n=\frac{2}{\pi n}\left[1-(-1)^n\right]. \tag{A9}$$

Fig. A1 shows a dependence of temperature $T(x,t)$ along the thermocouple length, obtained both by the Grinberg method [30] (TG), and by the method of separation of variables (TD) stated above. (Parameters of TE device correspond to those given in the paper).

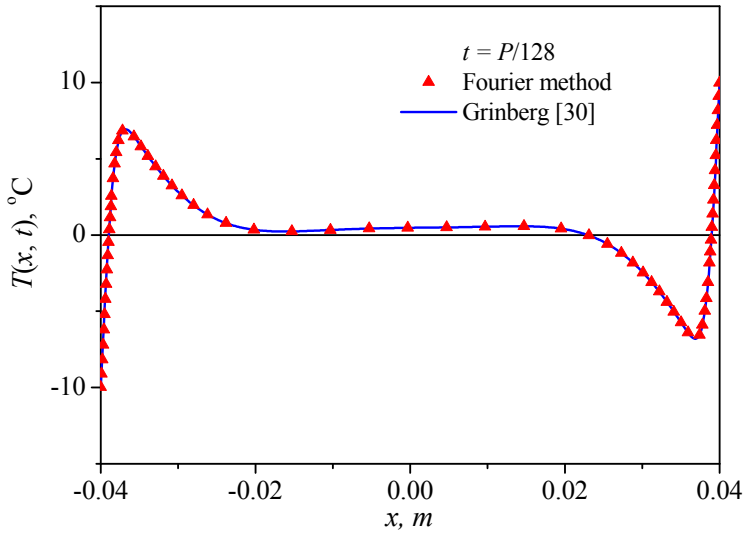

Fig. A1. As an example, temperature distribution along the thermocouple leg is given along thermocouple leg for time moment $t = P/128$, continuous line is solution by the Grinberg method [30], (19) triangles – by the method of separation of variables (A6).

As is evident from Fig. A1, temperature distribution $T(x,t)$ obtained by both methods – the method of separation of variables and the Grinberg method [30] practically coincide. For the calculation of the generation and cooling modules and for their optimization it is necessary to calculate heat fluxes, including the derivatives of temperature $\partial T/\partial x$ on the ends of thermocouple legs $x=\pm a$. For the solution obtained by the method of separation of variables such a derivative cannot be calculated, as long as for $x=\pm a$ formula (A9) gives a divergent series, whereas solution (19) obtained according to [30] at $x=\pm a$ converges, and the derivative can be calculated, see (20)-(22).

Fig. A2 shows a dependence of temperature $T(x,t)$ for different thermal diffusivity values. Coefficients λ_n are inversely proportional to thermal diffusivity (and, hence, thermal conductivity), thus, the higher λ_n, the deeper temperature variations will penetrate into a TE device leg.

Note that dependence 3 in Fig. A2 is given for thermal diffusivity value corresponding to the value of μ_0 (27) equal to 1.53, i.e. the one found in (56). Further thermal diffusivity increase does not change the form of dependence 3 in Fig. A2. With such thermal conductivity value heat fully comes to the middle of thermocouple leg, and the dependence $T(x,P/4)$ becomes fixed.

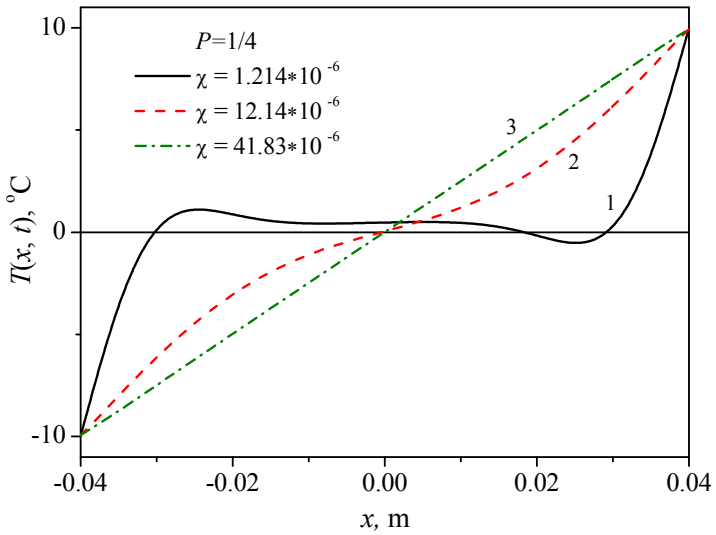

Fig. A2. Temperature distribution at time moment $P/4$ along thermoelement leg at different thermal diffusivity values 1 – $\chi = 1.214 \cdot 10^{-6}\, m^2/s$, 2– $\chi = 12.14 \cdot 10^{-6}\, m^2/s$, 3 – $\chi = 4.183 \cdot 10^{-5}\, m^2/s$.

Fig. A3 gives dependences $T(x,t)$ and $\partial T/\partial x$ at different time points. To calculate the derivative, the solution by the Grinberg method was used [30].

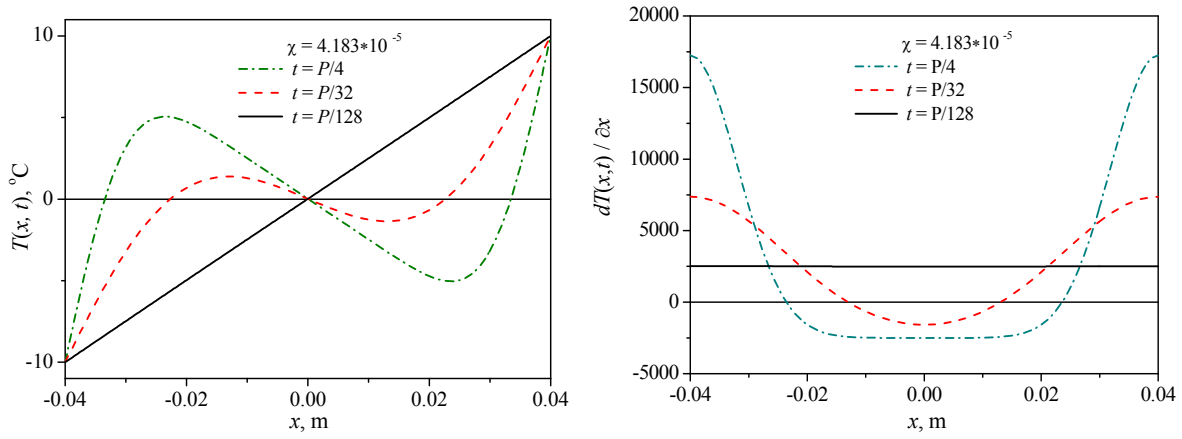

Fig. A3. Dependences of temperature T(x,t) (a) and temperature gradient $\partial T/\partial x$ (b) at time points $P/128$, $P/32$, $P/4$ for $\chi = 4.183 \cdot 10^{-5}\, m^2/s$.

As is seen from Fig. A3, that part of heat flux which is due to temperature gradient $\partial T / \partial x$ ($q_x = -\kappa \cdot \partial T / \partial x + \Pi j_x$) in the middle of thermocouple leg, close to $x = 0$, is much less that the flux on the ends, where there are large heat fluxes entering the hot end and coming into the cold end. In so doing, due to smallness of $\partial T / \partial x\big|_{x=0}$ there is practically no through flux through thermocouple leg.

References

1. T. M. Tritt, *Annual Review of Materials Research*, **41**, 433 (2011).
2. G. J. Snyder, and Eric S. Toberer, *Nature Materials* **7**, 105 (2008).
3. G. S. Nolas, J. Poon, and M. Kanatzidis, *Materials Research Society Bulletin*, **31**, 199 (2006).
4. H. Alam, S. Ramakrishna, *Nano Energy* **2**, 190 (2013).
5. G.S. Nolas, J. Sharp, and J. Goldsmid, *Thermoelectrics. Basic Principles and New Materials Developments*, Springer Series in Materials Science **45-VIII** (Springer-Verlag, Berlin, 2001), p.293.
6. X.F. Zheng, C.X. Liu, Y.Y. Yan, and Q. Wang, *Renewable and Sustainable Energy Reviews* **32,** 486 (2014).
7. *New Materials for Thermoelectric Applications: Theory and Experiment*, NATO Science for Peace and Security Series B: Physics and Biophysics, edited by V. Zlatic and A. Hewson (Springer, New York, 2013) p.273.
8. Properties and Applications of Thermoelectric Materials. The Search for New Materials for Thermoelectric Devices. *Proceedings of the NATO Advanced Research Workshop on Properties and Application of Thermoelectric Materials*, Hvar, Croatia, 21-26 September 2008, edited by V. Zlatic and A. Hewson, NATO Science for Peace and Security Series B: Physics and Biophysics (Springer, New York, 2009), p.340.
9. *Thermoelectric Nanomaterials Materials Design and Applications*. Springer Series in Materials Science, **182-XIX**, edited by K. Koumoto, T. Mori, (Springer, New York, 2013), p.387.
10. L. Weishu, Y. Xiao, C. Gang, and R. Zhifeng, *Nano Energy* **1**, 42 (2012).
11. L. P. Bulat, I. A. Drabkin, V. V. Karatayev V. B. Osvenskii, Yu. N. Parkhomenko, D. A. Pshenay-Severin, and A. I. Sorokin, *Journal of Electronic Materials*, **43**, 2121 (2014).
12. L. P. Bulat, V. B. Osvenskii, and D. A. Pshenai-Severin, *Physics of the Solid State*, **55**, 2442 (2013).
13. A. Snarskii, A. K. Sarychev, I. V. Bezsudnov, and A. N. Lagarkov, *Semiconductors*, 46, 659 (2012).
14. H. J. Goldsmid, *Introduction to Thermoelectricity*, Springer Series in Materials Science, **121**, (Springer, Berlin, 2009), p. 242.
15. Q. Zhou, Z. Bian, and A Shakouri, *J. Phys. D: Appl. Phys*. **40**, 4376 (2007).
16. G. J. Snyder, J.-P. Fleurial, T. Caillat, R. Yang, and G. Chen, *J. Appl. Phys*., **92**, 1564, (2002).
17. Yu. I. Dudarev, M. Z. Maksimov, *Technical Physics*, **43**, 737 (1998).
18. Chakraborty, K. C. Ng, *International Journal of Heat and Mass Transfer*, **49**, 1845 (2006).
19. R. Yanga, G. Chena, A. R. Kumarb, G. J. Snyder, and J.-P. Fleurial, *Energy Conversion and Management*, **46**, 1407 (2005).
20. J. N. Mao, H. X. Chen, H. Jia, and X.L. Qian, *Journal of Applied Physics*, **112**, 014514 (2012).
21. L. S. Stilbans, N. A. Fedorovich, *Sov. Phys.—Tech. Phys*. **3,** 460 (1958).
22. J. E. Parrott, *Solid State Electron*. **1,** 135 (1960).

23. V. A. Naer, *Journal of Engineering Physics*, **8**, 340 (1965).
24. E.K. Iordanishvili, *Thermoelectric Power Sources*, (Publ. Sov. Radio, Moscow, 1968), p.110
25. G. J. Snyder, J. P. Fleurial, T. Caillat, R. Yang, and G. Chen, *J. Appl. Phys*. **92,** 1564 (2002).
26. G. E. Hoyos, K. R. Rao, and D. Jerger, *Energy Convers*. **17,** 45 (1977).
27. K. Landecker, A.W. Findlay, *Solid State Electron*. **3,** 239 (1961).
28. T. Thonhauser, G.D. Mahan, L. Zikatanov, and J. Roe, *Appl. Phys*. Lett. **85,** 3247 (2004).
29. R. L. Field, H. A. Blum, *Energy Conversion*, **19-3**, 159 (1979).
30. G. A. Grinberg, *Selected Problems of Mathematical Theory of Electric and Magnetic Phenomena*. (Publ, Ac. of Sci. USSR, Moscow, 1948), p. 727.
31. R. Haberman, *Elementary Applied Partial Differential Equations with Fourier Series and Boundary Value Problems* (Englewood Cliffs, NJ: Prentice-Hall, 1998) p 215.
32. D. Zwillinger, Handbook of Differential Equations (3rd edition), (Academic Press, Boston, 1997) p.828.
33. D. Polyanin, V. F. Zaitsev, Handbook of Exact Solutions for Ordinary Differential Equations (2nd edition), (Chapman & Hall/CRC Press, Boca Raton, 2003), p.816.
34. Thermoelectrics Handbook. Macro to Nano, edited by D.M. Rowe (CRC Press, 2005) p.1014.

Submitted 11.09.14